coatings

MDPI

Article

Microstructure and Sliding Wear Resistance of Plasma Sprayed Al_2O_3-Cr_2O_3-TiO_2 Ternary Coatings from Blends of Single Oxides

Maximilian Grimm [1,*], Susan Conze [2], Lutz-Michael Berger [2], Gerd Paczkowski [1], Thomas Lindner [1] and Thomas Lampke [1]

[1] Materials and Surface Engineering Group, Institute of Materials Science and Engineering, Chemnitz University of Technology, D-09107 Chemnitz, Germany; gerd.paczkowski@mb.tu-chemnitz.de (G.P.); lindt@hrz.tu-chemnitz.de (T.L.); thomas.lampke@mb.tu-chemnitz.de (T.L.)

[2] Fraunhofer Institute for Ceramic Technologies and Systems, Fraunhofer IKTS, D-01277 Dresden, Germany; susan.conze@ikts.fraunhofer.de (S.C.); lutz-michael.berger@ikts.fraunhofer.de (L.-M.B.)

* Correspondence: maximilian.grimm@mb.tu-chemnitz.de; Tel.: +49-371-531-36581

check for updates

Abstract: Al_2O_3, Cr_2O_3, and TiO_2 are most commonly used oxide materials for thermal spray coating solutions. Each oxide shows unique properties comprising behavior in the spray process, hardness, corrosion, and wear resistance. In order to exploit the different advantages, binary compositions are often used, while ternary compositions are not studied yet. Atmospheric plasma spraying (APS) of ternary compositions in the Al_2O_3-Cr_2O_3-TiO_2 system was studied using blends of plain powders with different ratios and identical spray parameters. Coatings from the plain oxides were studied for comparison. For these powder blends, different deposition rates were observed. The microstructure, roughness, porosity, hardness, and wear resistance were investigated. The formation of the splats from particles of each oxide occurs separately, without interaction between the particles. The exception are the chromium oxide splats, which contained some amounts of titanium. The predominant oxide present in each blend has a decisive influence on the properties of the coatings. While TiO_x causes a low coating porosity, the wear resistance can be increased by adding Cr_2O_3.

Keywords: atmospheric plasma spraying; Al_2O_3; Cr_2O_3; TiO_2; microstructure; sliding wear; phase transformation; reactivity

1. Introduction

Thermally sprayed oxide ceramic coatings have an outstanding importance in many technological areas. Coatings sprayed from the single oxides and some commercially available binary compositions of the Al_2O_3-Cr_2O_3-TiO_2 system have multi-functional properties and are widely used as wear and as (sealed) corrosion resistant coatings. Depending on the composition, they are electrically insulating or conductive [1,2].

Plasma spraying and, in particular, conventional atmospheric plasma spraying (APS), is the most widely used thermal spray process for oxide coating manufacturing. Water stabilized plasma spraying (WSP) is a special high-energy process for coating manufacturing and is applied for special purposes, such as manufacturing of ceramic tubes. Coatings with excellent properties can be deposited by high velocity oxy-fuel spraying (HVOF), but often lower powder feed rates and deposition efficiencies are considered as drawbacks. More detailed descriptions of the spray processes used for oxide coating manufacturing are given elsewhere [2–4].

Most commonly feedstock powders with a typical particle size in the range 15–45 μm are used. The main feedstock powder manufacturing method for the single oxides is fusing and crushing.

For avoiding the formation of metallic chromium for Cr_2O_3 sintering and crushing is also common. For the commercially available binary compositions, the variety of the manufacturing methods are significantly broader. This includes mechanical blends of separately fused and crushed single oxide powders, jointly fused and crushed powders, but also agglomerated and sintered powders. Depending on the oxide particle or grain size, there are large differences in the homogeneity of mixing of the metallic elements in these methods. The homogeneity is lowest in case of the powder blends from single oxide powders and highest in the case of agglomerated and sintered powders, where finely dispersed oxide powders are mixed in the manufacturing process. Suspensions as feedstock become increasingly important, but are currently limited to single oxides [5]. Suspensions with two components are under investigation [6].

Each of the single oxides shows a specific material behavior during spraying, which is detrimental to the processing and/or coating properties [1,2].

For alumina, the detrimental phase transformation from α-Al_2O_3 (corundum) existing in the feedstocks to metastable phases, predominantly γ-Al_2O_3, in the coatings is well known [7–10]. The reason is the high cooling rate and nucleation of undercooled melt. Some content of the remaining α-Al_2O_3 in the coating is usually explained by the occurrence of non-molten particles [7]. An increase of the α-Al_2O_3 content in the coatings is described as an important measure to improve the coating properties, such as wear, electrical, and corrosion resistance. Except the addition of other oxides (e.g., Cr_2O_3 [8–10]), there are several technological measures for this, as the selection of special spray process conditions [11], use of suspensions [1,5] or heat post-treatments [12] as well as plasma-electrolytic oxidation of arc-sprayed and flame-sprayed aluminum coatings [13]. However, each of these technological measures has certain limitations and the stabilization of the α-Al_2O_3 by a tailored powder would be favored.

Chromia has a low deposition efficiency due to oxidation from Cr_2O_3 to volatile CrO_3, which immediately reconverts to Cr_2O_3 when cooling down [1,2,14]. Formation of Cr(VI)-oxyhydrates in wet atmospheres is another detrimental reaction [14,15]. Although the appearance of hexavalent chromium is below the maximum allowable concentrations under normal process conditions, increased safety regulations are permanently under discussion. By adding Al_2O_3 [16] or TiO_2 [1,2] to Cr_2O_3 and forming respective solid solutions, both the formation of hexavalent chromium is suppressed and the deposition efficiency is increased.

Since titania TiO_2 readily loses oxygen in a reducing environment such as during the fusion step of feedstock manufacturing, fused and crushed feedstock powders are non-stoichiometric and preferably designated as TiO_x. The oxygen content can also change during the spray process. The oxygen defects are often disordered in coatings under the strong nonequilibrium conditions of the thermal spray process, but also often forms ordered-structures for certain O/Ti ratios (Magnéli-phases) in feedstock powders, manufactured with lower cooling rates. Due to a eutectic with an oxygen content corresponding to x of about 1.78 in the Ti-O phase diagram (in the two-phase region of the Magnéli-phases Ti_4O_7 and Ti_5O_9). The temperature of appearance of a melt is decreased from 1857 °C for TiO_2 down to 1679 °C at the eutectic point [2,17].

It was found that the addition of a second oxide can improve the coating properties [1,2]. There are some indications in the literature that the coating properties can be further improved by ternary compositions and by the addition of the third oxide of the system. Examples of such potential improvements can be the stabilization of target phases, an acceleration of the formation of a compound and improved sintering properties. This can relate to the feedstock powder manufacturing step and/or the spray process.

This addition can be made in different ways, e.g., during the feedstock manufacturing process (joint processing in fused and crushed as well as agglomerated and sintered powder manufacturing) or by blending single oxide powders. The latter case is the simplest one, and blended powders have a high importance in the current industrial practice of thermal spraying. This is valid for commercially available blends in the Al_2O_3-TiO_2 system, such as Al_2O_3-40%TiO_2 and Al_2O_3-13%TiO_2 [18,19], but also

for blending at the production site [20]. In general, an interaction between components of the blends will occur only during the spray process and is, in general, expected to be low due to the large particle size. However, an intensive interaction during the spray process was found in the case of an Al_2O_3-40%TiO_2 blend [21]. Another example are blends of alumina-rich compositions of the Al_2O_3-Cr_2O_3 system, which can lead to a stabilization of the α-Al_2O_3 during WSP [10]. Blends of the binary Cr_2O_3-TiO_2 system were investigated as well [17,20]. However, ternary compositions of the Al_2O_3-Cr_2O_3-TiO_2 system were not studied neither as powder blends, pre-alloyed powders, nor suspensions.

In this work, the interaction of single oxide ternary powder blends of the Al_2O_3-Cr_2O_3-TiO_2 system during APS and their sliding wear properties are studied. Coatings from the single oxides are investigated for comparison.

2. Materials and Methods

Commercial fused and crushed Al_2O_3, Cr_2O_3, and TiO_x powder grades, compiled in Table 1, were used in this work. The particle size distribution was determined by laser diffraction analysis in a Cilas 930 device (Cilas, Orléans, France). To prepare the powder blends, dried powders were mixed using a tumble mixer, according to the compositions given in Table 2.

Table 1. Commercial single oxide feedstock powder grades, their particle size given by the supplier, and their granulometric data (own measurement). All powders were produced by fusing and crushing.

Material	Supplier	Particle Size	Granulometric Data		
			d_{10}	d_{50}	d_{90}
Al_2O_3	Saint Gobain Coating Solutions, Avignon, France	$-45 + 15$ μm	21	34	56
Cr_2O_3	GTV, Luckenbach, Germany	$-45 + 15$ μm	19	34	54
TiO_x	Ceram, Albbruck-Birndorf, Germany	$-45 + 20$ μm	22	39	61

Table 2. Compositions of the powder blends.

Designation of the Blend/Coating	Components (at %)			Components (wt %)		
	Al_2O_3	Cr_2O_3	TiO_2	Al_2O_3	Cr_2O_3	TiO_2
ACT	50	25	25	47	35	18
CAT	25	50	25	21	63	16
TAC	25	25	50	25	36	39

Feedstock powders were investigated with a scanning electron microscope (SEM) LEO 1455VP (Zeiss, Jena, Germany) with an acceleration voltage of 25 kV. By using a backscattered electron detector (BSD), the material contrast is visualized by different grey levels. In addition, phase composition was studied by X-ray diffraction (XRD) using a Bragg-Brentano geometry operating with Cu K_α radiation with a D8 Advance diffractometer (Bruker AXS, Billerica, MA, USA) in a range of $2\theta = 15°$–$120°$ with a step size of $0.02°$ and 3 s/step.

Low carbon steel (S235) samples with a diameter of 40 mm were used as substrates, which were grit blasted with alumina (EK-F 24) (3 bar, 20 mm distance, 70° angle) and cleaned in an ultrasonic ethanol bath before applying the coating. The coatings were produced by atmospheric plasma spraying using an F6 torch (GTV, Luckenbach, Germany) and the spraying parameters, according to Table 3. In order to ensure good comparability, all coatings in this work were sprayed with this parameter set. The parameter set was chosen in such a way that a shift of the composition of the powder blends during processing was avoided. Interruptions of the coating process ensured that the substrate did not heat up to more than 200 °C.

The cross sections of the coatings were prepared by the standard metallographic procedure. The analysis of the microstructure was conducted using an optical microscope GX51 (Olympus, Shinjuku, Japan) equipped with a SC50 camera (Olympus, Shinjuku, Japan) as well as by SEM with the

same device used for powder analysis. The coating thickness was ascertained at 10 evenly distributed points. To determine the porosity, five images of the coating were evaluated by the image analysis method with the software ImageJ. Furthermore, the hardness of the coatings was measured on the cross sections using a Wilson Tukon 1102 device (Buehler, Uzwil, Switzerland). For this purpose, 10 Vickers indentations with a test load of 2.94 N were examined. The XRD patterns of the coatings were recorded with 3003 TT diffractometer from GE Inspection Technologies in a range of $2\theta = 15°–80°$ with a step size of $0.03°$ and 4 s/step. The high-resolution microstructure and the local chemical composition of individual splats in the coatings from blends were determined using a FESEM Ultra (Zeiss, Jena, Germany) equipped with an EDS detector X-Max80 and using a voltage of 13 kV. At least five measurements for the three typical individual splat compositions in each coating were performed. The calibration for the quantitative EDS analyses were performed using a cobalt standard.

Table 3. The parameters of the APS process with the F6-torch.

Argon	Hydrogen	Current	Spraying Distance	Traverse Speed	No. of Passes	Powder Feed Rate
41 L/min	11 L/min	600 A	110 mm	0.4 m/s	10	30 g/min

The processing of the coatings by grinding and polishing was investigated. All coated samples were simultaneously ground on grinding wheels up to a number of 1200 for 3 min at 300 rpm and 25 N. Polishing was then carried out with diamond suspensions down to 1 µm at 200 rpm and a slightly reduced force in order to obtain comparable surfaces for the wear tests. The roughness of as-sprayed and ground coatings was recorded with a tactile profilometer (Jenoptik, Jena, Germany) with five measuring tracks. The characterisation of the sliding wear behavior of the coatings was carried out using a ball on disc test (Tetra, Ilmenau, Germany) using the parameters summarized in Table 4. For each coating, three wear tracks were generated. The evaluation of the wear tracks with regard to the wear depth and the wear volume was carried out using a 3D profilometer MikroCAS (LMI, Teltow, Germany).

Table 4. Ball-on-disk test parameters.

Force	Radius	Speed	Cycles	Wear Distance	Counter Body	
					Material	Diameter
10 N	5 mm	0.05 m/s	15916	500 m	Al_2O_3	6 mm

3. Results

3.1. Feedstock Powder Characterisation

The typical angular morphology of the fused and crushed powder particles is shown in the SEM micrograph in Figure 1. The granulometric parameters d_{10}, d_{50}, and d_{90}, which are also given in Table 1, confirm only minor differences of their particle sizes, which makes them suitable for blending.
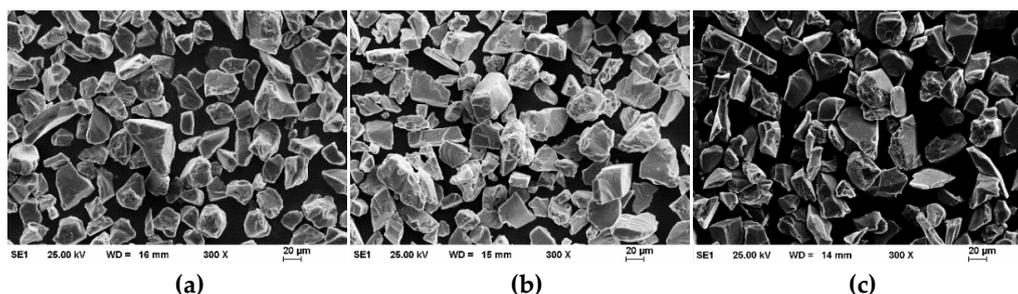

Figure 1. SEM images of the feedstock powders. (**a**) Al_2O_3. (**b**) Cr_2O_3. (**c**) TiO_x.

According to the XRD measurements, as shown in Figure 2, the alumina and chromia feedstock powders consist only of α-Al$_2$O$_3$ (corundum) and Cr$_2$O$_3$ (eskolaite), respectively. In the SEM investigation of the chromia powder, small amounts of metallic chromium were detected, which do not appear in the XRD pattern. A large number of peaks in addition to those of rutile were detected for the TiO$_x$ powder. These additional peaks, which are not labelled in the pattern in Figure 2, belong to substoichiometric titanium oxide phases. The presence of the (110) peak of rutile at $2\theta = 27.4°$ indicates that local concentrations of oxygen are closed to stoichiometry, while, in other regions, disordered oxygen-deficient structures exist. According to the gravimetric measurements in another study, x in TiO$_x$ powder is about 1.9 [19].
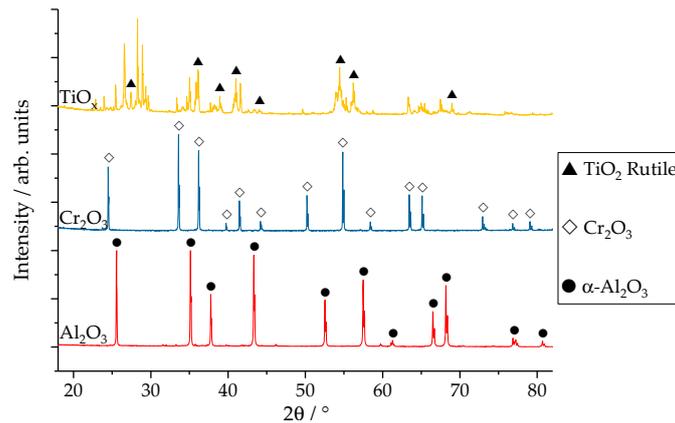
Figure 2. XRD pattern of the feedstock powders.

3.2. Coating Characterisation

It was shown that, with the selected parameter set, it was possible to produce well adhering and dense coatings from all single oxides and their ternary blends. The results of the roughness measurements for the as-sprayed coatings shown in Figure 3 reveal clear differences. In the case of single oxides, the TiO$_x$ coating has the highest as-sprayed *Rz* value with approximately 70 ± 2 µm. The Cr$_2$O$_3$ coatings show the lowest roughness with approximately 33 ± 2 µm. Coatings produced from the powder blends show roughness values between these limits. The as-sprayed Rz value of the ACT, CAT, and TAC coatings are 50 ± 4 µm, 49 ± 3 µm, and 55 ± 6 µm, respectively. By grinding and polishing the roughness of the samples, it can be reduced by more than 90%. As can be seen in Figure 3, the Rz values after polishing are in the range of 1.3 ± 0.2 µm for Cr$_2$O$_3$ and 3.2 ± 0.2 µm for Al$_2$O$_3$. The roughness of the TiO$_x$ coating can even be reduced by almost 98% by polishing and indicates particularly good machinability. The coatings from the blends show a similar behavior. The Cr$_2$O$_3$-rich CAT coating with 2.3 ± 0.5 µm have the lowest roughness. After polishing, all coatings have a comparable roughness, which makes them suitable for wear testing.
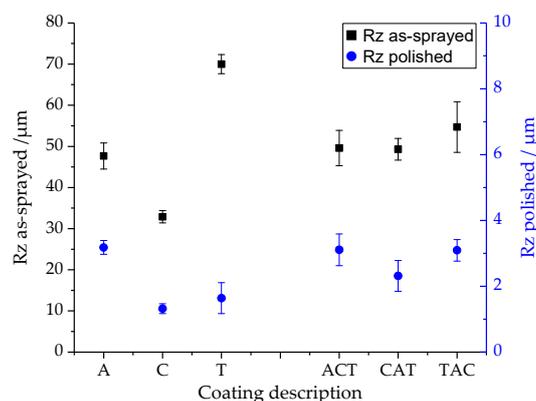

Figure 3. Roughness values of as-sprayed and polished coated samples.

The results of coating thickness and porosity after 10 passes are shown in Figure 4. The coating thickness gives an indication of the deposition rate of the single oxides and the blends. In the case of the individual oxides, the highest coating thickness (469 ± 16 μm) was measured for the TiO$_x$ coating, while the chromia coating has the lowest coating thickness. A similar observation was made by others [17]. For the coatings from the blended powders, the titanium oxide-rich TAC coating with 430 ± 18 μm shows significantly higher thickness than the ACT and CAT coatings, where the coating thickness is 342 ± 14 μm and 369 ± 16 μm, respectively.
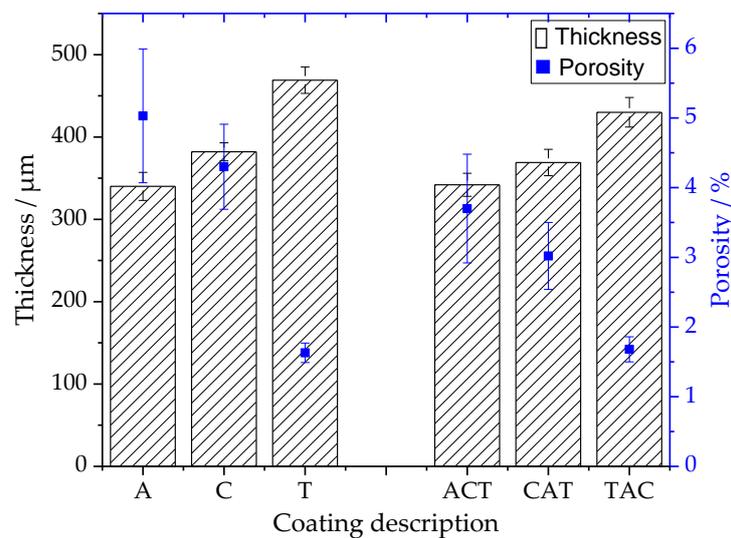
Figure 4. Thickness and porosity of plain oxide coatings (A, C, T) and coatings from blends (ACT, CAT, and TAC).

When studying the porosity, it is noticeable that different levels exist between the individual oxides as a result of the identical spray parameters. While the porosity of the Al$_2$O$_3$ coating is about 5.0% ± 1.0%, the TiO$_x$ coating with a porosity of 1.6% ± 0.1% is significantly denser. As illustrated in Figure 4, the alumina-rich ACT and chromium oxide-rich CAT coatings have similar porosities of 3.7% ± 0.8% and 3.0% ± 0.5%, respectively. Only the TAC coating with a high content of TiO$_x$ shows a lower porosity of 1.7% ± 0.2%.

Low magnification SEM images of the cross sections of the coatings from the blends are shown in Figure 5a,c,e. The characteristic microstructure of thermal spray coatings, characterized by unmolten particles, pores, microcracks, and a lamellar structure, is observed. Splats from the individual oxide particles are clearly distinguishable. The high magnification images in Figure 5b,d,f show that the coatings of each blend consist of individual splats of a comparable grayscale denoted as I, II, and III in each of the images.

The results of the measurements of local chemical composition of these individual splats by EDS are compiled in Figure 6. The dark areas (SEM area I) in all coatings have a composition of approximately 60 at % oxygen and 40 at % aluminum, while the elements titanium and chromium were not detected. The bright areas (SEM area II) assigned to Cr$_2$O$_3$ contain a significant proportion of titanium in the range between 0.9 at %. and 2.2 at %. It is also noticeable that these Cr$_2$O$_3$ lamellae contain more oxygen than expected (slightly above 60 at %). Variations in the grayscales in these lamellas were found to be caused by variations of the oxygen content. The areas III with an intermediate grayscale relate to the titanium oxide splats.
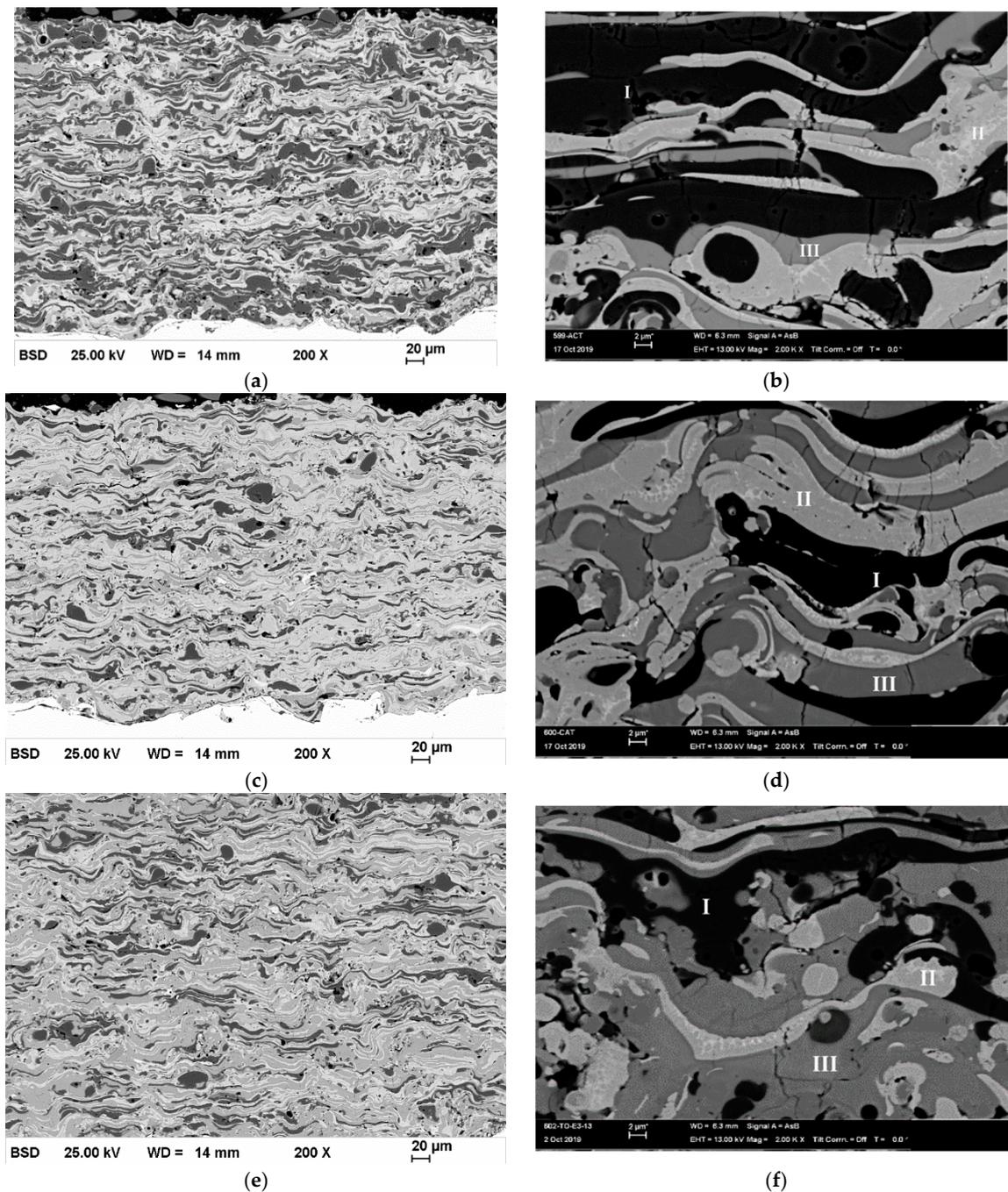
Figure 5. SEM images (BSD detector) of APS Al_2O_3-Cr_2O_3-TiO_2 composite coatings: top row: ACT-coating: (**a**) overview image, (**b**) detailed image with marked areas for the EDS measurement. middle row: CAT-coating: (**c**) overview image, (**d**) detailed image with marked areas for the EDS measurement. bottom row: TAC-coating: (**e**) overview image, (**f**) detailed image with marked areas for the EDS measurement. The EDS measurements of the marked areas are shown in Figure 6.

The results of the hardness measurements are presented in Figure 7 and show that all single oxide coatings have high hardness values above 1000 HV0.3, while the Cr_2O_3 coating has the highest hardness of 1250 ± 79 HV0.3. The coatings from powder blends do not reach the hardness of the plain chromia and alumina coatings. Only the chromium oxide-rich CAT coating has a hardness of 1074 ± 65 HV0.3, which is higher than the hardness of the TiO_x coating. The lowest hardness was found for the ACT coating.
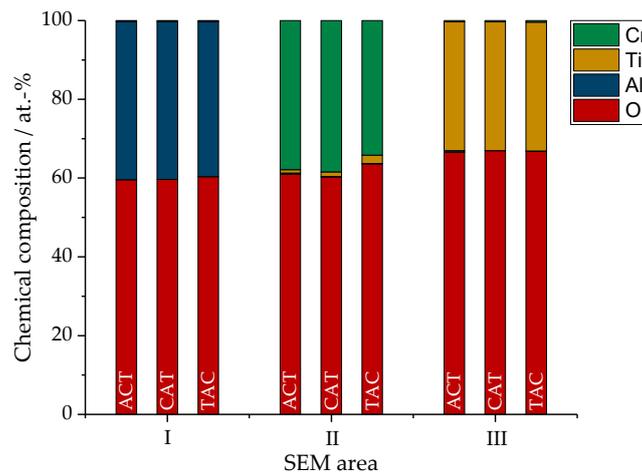
Figure 6. EDS analysis of composite coatings: chemical composition of the material areas marked in Figure 5b,d,f.
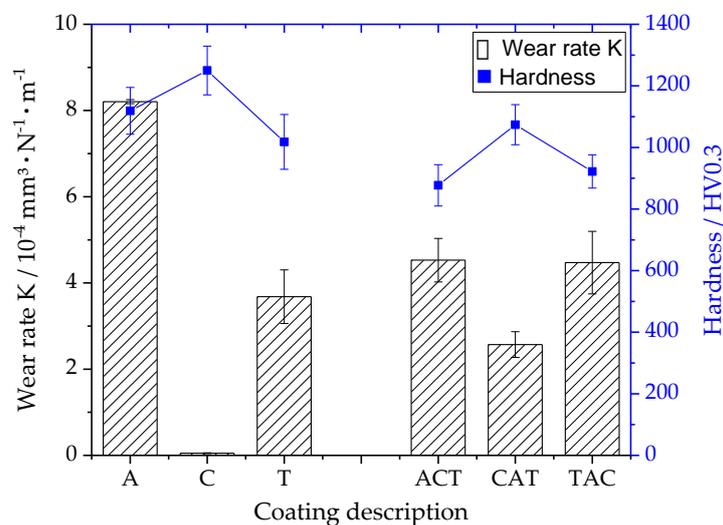

Figure 7. Hardness and sliding wear rates of plain oxide coatings (A, C, T) and composite coatings (ACT, CAT, TAC).

The results of the sliding wear tests are also shown in Figure 7. The Al_2O_3 coating shows the highest wear rate ($8.2 \pm 0.1 \times 10^{-4}$ $mm^3 \cdot N^{-1} \cdot m^{-1}$), which is more than twice than that of the TiO_x coating. The wear resistance of the chromium oxide coating is so high that no meaningful wear rate was measured. The coatings from the blends also show a high wear resistance. The ACT and TAC coatings have a very similar wear rate. The chromium oxide-rich CAT coating proves to be more wear resistant.

The presentation of the XRD patterns, displayed in Figure 8, is limited to the range $2\theta = 18°–82°$. For the powder blends, the presence of α-Al_2O_3 (corundum), Cr_2O_3 (eskolaite), and different titanium oxide phases, as expected from the pattern of the individual oxides (see Figure 2) was found. The XRD patterns of the coatings from the blends, shown in Figure 8, reveal the presence of α-Al_2O_3, γ-Al_2O_3, Cr_2O_3 (eskolaite), and different titanium oxide phases. A shift of the peak positions relative to the standards did not occur. Due to the inhomogeneous distribution of oxygen, the intensity of the suboxide peaks is low. A quantitative determination of the phase is not possible. A change in the intensity of some peaks was observed. For the TAC coating, the TiO_x peaks of $2\theta = 26°–30°$ lose significantly in intensity in the coating compared to the powders. The intensity of the TiO_2 rutile peaks at $2\theta = 27.4°$ (110) and $2\theta = 54.2°$ (211) increases markedly. For all coatings, especially for the CAT and TAC coatings, a decrease of peak intensity of α-Al_2O_3 from powder to coating was detected.
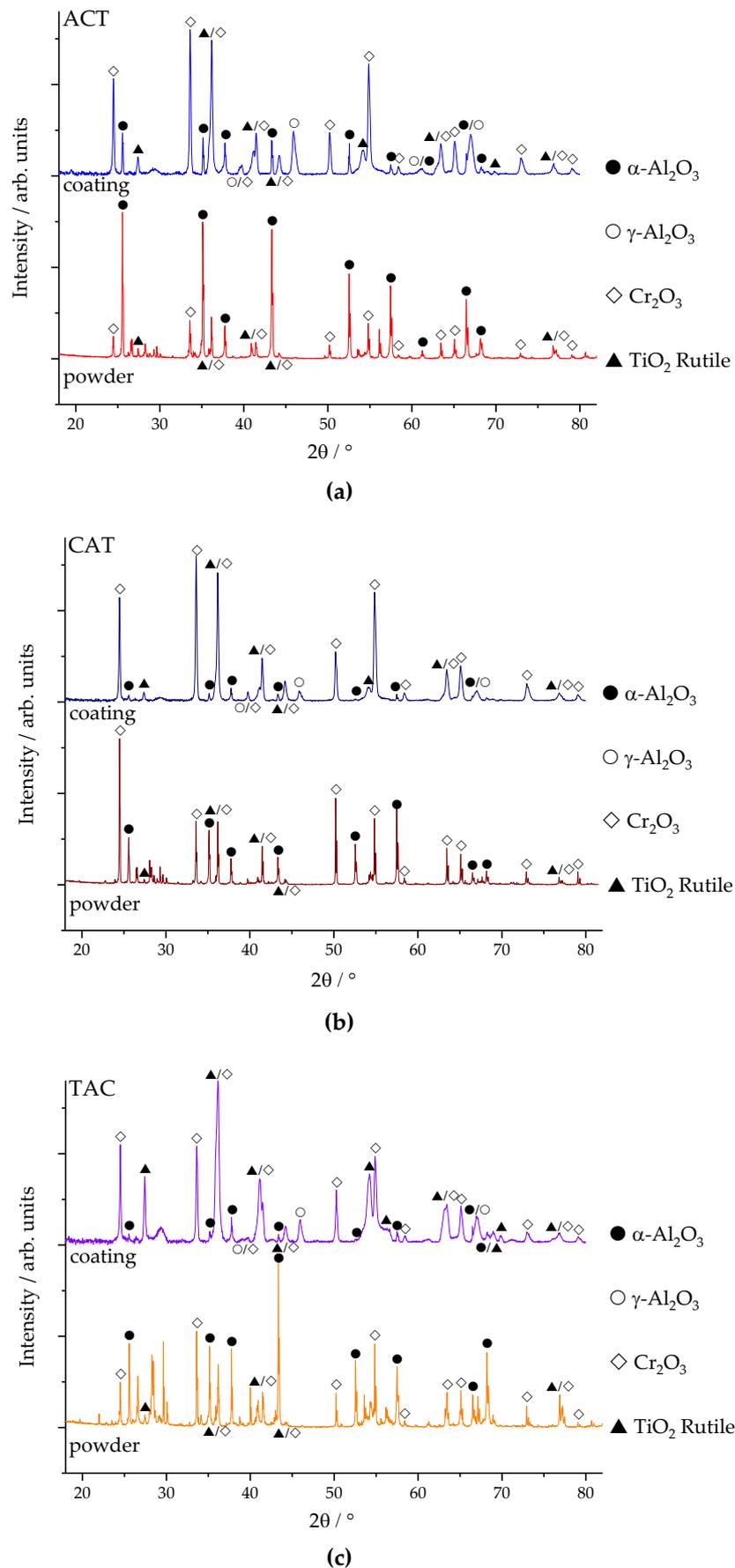
**Figure 8.** Diffraction patterns of the powder blends and corresponding coatings: (**a**) ACT, (**b**) CAT, and (**c**) TAC.

4. Discussion

Spraying of blends containing large powder particles has the disadvantage that only one component can be sprayed with a truly optimized parameter set. For ternary blends, this is naturally even more difficult as for binary ones. By this reason, for this study, an identical parameter set was used, which represents a compromise for the processability of all oxides. In case of the blends of the Al_2O_3-Cr_2O_3-TiO_2 system, two high melting components (Al_2O_3 and Cr_2O_3) are combined with one lower melting oxide TiO_x. Thus, the liquid phase occurs at lower temperatures compared to TiO_2 and the addition of TiO_x to Cr_2O_3 and Al_2O_3 decreases the coating porosity. For Al_2O_3-rich and Cr_2O_3-rich powder blends (ACT and CAT), a part of the large particle fraction is not melted to the extent that it can contribute to coating build up due to the higher melting temperature. As indicated by the coating thickness after 10 passes (see Figure 4), the highest deposition efficiency is found for the TAC coating.

The XRD investigations show that the typical phase transformation from α-Al_2O_3 to γ-Al_2O_3 as described in Section 1 occurs for all powder blends. The additions of Cr_2O_3 and TiO_2 for the given spray conditions do not have an effect on this phase transformation, which aligns with the literature data [2]. In addition, reduced peak intensities related to sub-stoichiometric phases and an increase of the rutile peaks intensity at $2\theta = 27.4°$ (110) and $2\theta = 54.2°$ (211) can be an indication for oxygen gain during the processing and formation of stoichiometric TiO_2 or near stoichiometric TiO_x as a result of the thermal spray process.

Recently, a surprising high dissolution of titanium atoms in γ-Al_2O_3 in APS coatings obtained from a commercial Al_2O_3-40% TiO_2 powder blend was observed [19]. Surprisingly, this was not observed in this study for any of the ternary blends.

In the literature, the formation of a Cr_2O_3-rich solid solution $(Cr,Ti)_2O_3$ is described for binary suspensions [14], while, for blends of large particles, contradictory results are reported [17,20]. In this study, the EDS measurements have shown the presence of small amounts of titanium in the chromium oxide lamellae. The titanium content in the chromia splats of the ACT and TAC coatings was below 2 at % but is slightly higher in the TiO_x-rich TAC coating. The higher titania content increases the number of interfaces between titanium and chromium oxide splats. Therefore, more titanium diffuses into the chromium oxide lamellae.

Since the hardness of the Cr_2O_3 coating was the highest, it is not surprising that the hardness is increased with a rising content of Cr_2O_3. The Cr_2O_3-rich CAT coating shows the highest hardness for the ternary blends. As expected, the Al_2O_3-rich ACT coating and the plain Al_2O_3 coating show higher hardness values than TiO_2-rich coatings. However, the titanium oxide-rich TAC coating has a similar hardness compared to the ACT coating. The lower porosity of the TAC coating is assumed to be responsible for this effect.

The sliding wear rate of Al_2O_3 coatings can be significantly reduced by adding TiO_x and Cr_2O_3. Both coatings have a higher wear resistance than the plain Al_2O_3 coating. Possible reasons could be the improved toughness of the coating expected by adding TiO_x [21] and/or addition of Cr_2O_3, which has, by far, the highest wear resistance. Except for the Al_2O_3 coating, coating hardness and sliding wear rates show some correlation especially for coatings from the blends. Whereas ACT and TAC coatings have similar hardness values and wear rates, the higher content of Cr_2O_3 in the CAT coating leads to significantly higher hardness values and a reduction in the wear rate. It should also be taken into account that the sliding wear rates of the plain oxide could be influenced by the identical spray parameter set, which is applied to the deposition of all coatings in this study.

All investigations reveal that the individual properties of the plain oxide strongly influence the properties of the coating from the blends. Therefore, for example, increasing the TiO_x content leads to denser coatings and higher deposition rates as well as higher as-sprayed roughness. The increase of the Cr_2O_3 content positively influences the sliding wear resistance.

5. Summary and Conclusions

It was shown that firmly adhering coatings can be produced by atmospheric plasma spraying from powder blends containing Al_2O_3, Cr_2O_3, and TiO_2 using an identical spray parameter set. Investigations with XRD have shown that the phase transformation from α-Al_2O_3 to γ-Al_2O_3 also occurs in the powder blends and is not influenced by the addition of Cr_2O_3 or TiO_x. Furthermore, for titania, a gain of oxygen content was found. EDS measurements have shown the existence of small amounts of titanium in the chromium oxide lamellaes. The investigations have shown that the respective dominant single oxide has a significant influence on the coating properties. Whereas a high TiO_x content leads to higher deposition rates, higher as-sprayed roughness, and low porosities, the hardness and wear resistance of the coatings can be improved by increasing the Cr_2O_3 content. By using powder blends, the sliding wear rate can be improved when compared to plain Al_2O_3 coatings. Thus, the use of powder blends presents a promising approach to adapt or extend the property profile of plain oxide coatings. The reactivity between the materials involved needs to be further investigated in order to exploit further improvement potentials.

References

1. Berger, L.-M.; Toma, F.-L.; Scheitz, S.; Trache, R.; Börner, T. Thermisch gespritzte Schichten im System Al_2O_3-Cr_2O_3-TiO_2—ein Update. *Mater. Werkst.* **2014**, *45*, 465–475. [CrossRef]
2. Berger, L.-M. Tribology of Thermally Sprayed Coatings in the Al_2O_3-Cr_2O_3-TiO_2 System. In *Thermal Sprayed Coatings and Their Tribological Performances*; Roy, M., Davim, J.P., Eds.; Engineering Science Reference: Hershey, PA, USA, 2015; pp. 227–267. [CrossRef]
3. Fauchais, P.L.; Heberlein, J.V.R.; Boulos, M.I. *Thermal Spray Fundamentals: From Powder to Part*; Springer: New York, NY, USA; Heidelberg, Germany; Dordrecht, The Netherlands; London, UK, 2014. [CrossRef]
4. Pawlowski, L. *The Science and Engineering of Thermal Spray Coatings*, 2nd ed.; Wiley: Hoboken, NJ, USA, 2008.
5. Toma, F.-L.; Potthoff, A.; Berger, L.-M.; Leyens, C. Demands, Potentials, and Economic Aspects of Thermal Spraying with Suspensions: A Critical Review. *J. Therm. Spray Technol.* **2015**, *24*, 1143–1152. [CrossRef]
6. Potthoff, A.; Kratzsch, R.; Barbosa, M.; Kulissa, N.; Kunze, O.; Toma, F.-L. Development and Application of Binary Suspensions in the Ternary System Cr_2O_3-TiO_2-Al_2O_3 for S-HVOF Spraying. *J. Therm. Spray Technol.* **2018**, *27*, 710–717. [CrossRef]
7. McPherson, R. On the formation of thermally sprayed alumina coatings. *J. Mater. Sci.* **1980**, *15*, 3141–3149. [CrossRef]
8. Chráska, P.; Dubsky, J.; Neufuss, K.; Pisacka, J. Alumina-base plasma-sprayed materials part I: Phase stability of alumina and alumina-chromia. *J. Therm. Spray Technol.* **1997**, *6*, 320–326. [CrossRef]
9. Dubsky, J.; Chraska, P.; Kolman, B.; Stahr, C.C.; Berger, L.-M. Phase formation control in plasma sprayed alumina-chromia coatings. *Ceram. Silik.* **2011**, *55*, 294–300.
10. Stahr, C.C.; Saaro, S.; Berger, L.-M.; Dubský, J.; Neufuss, K.; Herrmann, M. Dependence of the stabilization of α-Alumina on the spray process. *J. Therm. Spray Technol.* **2007**, *16*, 822–830. [CrossRef]
11. Heintze, G.N.; Uematsu, S. Preparation and structures of plasma-sprayed γ- and α-Al_2O_3 coatings. *Surf. Coat. Technol.* **1992**, *50*, 213–222. [CrossRef]

12. Marple, B.R.; Voyer, J.; Béchard, P. Sol infiltration and heat treatment of alumina-chromia plasma-sprayed coatings. *J. Eur. Ceram. Soc.* **2001**, *21*, 861–868. [CrossRef]

13. Lampke, T.; Meyer, D.; Alisch, G.; Nickel, D.; Scharf, I.; Wagner, L.; Raab, U. Alumina coatings obtained by thermal spraying and plasma anodising—A comparison. *Surf. Coat. Technol.* **2011**, *206*, 2012–2016. [CrossRef]

14. Toma, F.-L.; Potthoff, A.; Barbosa, M. Microstructural Characteristics and Performances of Cr_2O_3 and Cr_2O_3-15%TiO_2 S-HVOF Coatings Obtained from Water-Based Suspensions. *J. Therm. Spray Technol.* **2018**, *27*, 344–357. [CrossRef]

15. Yu, S.H.; Wallar, H. Chromia Spray Powders and a Process for Making the Same. U.S. Patent 6,774,076, 10 August 2004.

16. Richter, A.; Berger, L.-M.; Conze, S.; Sohn, Y.J.; Vaßen, R. Emergence and impact of Al_2TiO_5 in Al_2O_3-TiO_2 APS coatings. In Proceedings of the IOP Conference Series: Materials Science and Engineering 21th Chemnitz Seminar on Materials Engineering, Chemnitz, Germany, 6–7 March 2019; Volume 480, p. 012007. [CrossRef]

17. Sert, Y.; Toplan, N. Tribological behavior of a plasma-sprayed Al_2O_3-TiO_2-Cr_2O_3 coating. *Mater. Tehnol.* **2013**, *47*, 181–184.

18. Vernhes, L.; Bekins, C.; Lourdel, N.; Poirier, D.; Lima, R.S.; Li, D.; Klemberg-Sapieha, J.E. Nanostructured and Conventional Cr_2O_3, TiO_2, and TiO_2-Cr_2O_3 Thermal-Sprayed Coatings for Metal-Seated Ball Valve Applications in Hydrometallurgy. *J. Therm. Spray Technol.* **2016**, *25*, 1068–1078. [CrossRef]

19. Richter, A.; Berger, L.-M.; Sohn, Y.J.; Conze, S.; Sempf, K.; Vaßen, R. Impact of Al_2O_3-40 wt.% TiO_2 feedstock powder characteristics on the sprayability, microstructure and mechanical properties of plasma sprayed coatings. *J. Eur. Ceram. Soc.* **2019**, *39*, 5391–5402. [CrossRef]

20. Ctibor, P.; Píš, I.; Kotlan, J.; Pala, Z.; Khalakhan, I.; Štengl, V.; Homola, P. Microstructure and properties of plasma-sprayed mixture of Cr_2O_3 and TiO_2. *J. Therm. Spray Technol.* **2013**, *22*, 1163–1169. [CrossRef]

21. Fervel, V.; Normand, B.; Coddet, C. Tribological behavior of plasma sprayed Al_2O_3-based cermet coatings. *Wear* **1999**, *230*, 70–77. [CrossRef]